Journal of Intelligent Material Systems and Structures

Integrated Structural/Control Design of Micro-Positioner for Boring Bar Tool Insert

George P. O'Neal, Byung-Kwon Min, Zbigniew J. Pasek and Yoram Koren

The online version of this article can be found at:

Published by:

⑤SAGE

Additional services and information for *Journal of Intelligent Material Systems and Structures* can be found at:

Email Alerts: http://jim.sagepub.com/cgi/alerts

Subscriptions: http://jim.sagepub.com/subscriptions

Reprints: http://www.sagepub.com/journalsReprints.nav

Permissions: http://www.sagepub.com/journalsPermissions.nav

Citations: http://jim.sagepub.com/content/12/9/617.refs.html

Integrated Structural/Control Design of Micro-Positioner for Boring Bar Tool Insert

GEORGE P. O'NEAL, BYUNG-KWON MIN,* ZBIGNIEW J. PASEK AND YORAM KOREN

Department of Mechanical Engineering, The University of Michigan, 2250 Hayward St., 2250 GGB
Ann Arbor, Michigan, USA 48109-2125

ABSTRACT: This paper presents a method to improve the performance of an electro-mechanical system by employing an integrated structural/control design methodology. In their previous work, the authors have introduced an intelligent boring bar, utilizing a micro-positioner (composed of a piezoelectric actuator and photosensitive detectors) to actively control a cutting insert. The purpose of the micro-positioner was to improve precision of boring process by isolating the boring tool from tool vibrations and compensating tool position for geometric errors. The controller for the micro-positioner was designed only after the mechanical design was finalized. As a result, the controller performance was acceptable, but overall performance of the system was limited by its mechanical structure.

This paper introduces a new approach of concurrent design of the mechanical structure and the controller to enhance the performance of the micro-positioner. With the proposed method, both mechanical and control design variables are determined simultaneously in a single optimization problem. The objective and constraint equations quantify system performance, stability, actuator saturation, and life expectancy as explicit functions of the design variables. The proposed integrated methodology both simplifies the design process of the prototype boring tool and enhances its performance over the previous design, as shown by simulation results.

INTRODUCTION

EARLIER work by the authors (O'Neal et al., 1998) describes the development of a new boring tool called the *Smart Tool*. This tool utilizes a piezoelectric actuator and two laser photo sensors to actively isolate the cutting insert from erroneous bar motion while rejecting cutting force disturbances. Boring bars are metal cutting tools used to machine precision holes which are usually characterized by length-to-diameter (L/D) ratios. One end of the tool is typically fixed to a rotating spindle, while a cutting insert is attached to the free end; multiple supports and inserts are often used. Boring bars with large L/D ratios typically have low dynamic stiffness, leaving them susceptible to mechanical vibrations. Excessive vibrations reduce part quality and tool life. A significant amount of research effort and many applications have focused on developing methods to limit unwanted vibration in cutting operations, which would facilitate for boring at large L/D ratios.

The original *Smart Tool* design was carried out with a traditional design methodology: that is, the controller design was subsequent to that of the structural components. However, the *Smart Tool* operation is based on significant interaction between active and structural (passive) elements, resulting in nontrivial tradeoffs between the structural and controller design. Many of these tradeoffs are best handled with closed-loop analysis. The initial design process for the *Smart Tool* was hampered by a design methodology that did not assume an integrated approach. For example, traditionally fatigue has been considered as a structural phenomenon, and thus, effects of closed-loop control response from different control designs on a moving component were ignored.

Recently, there has been a great deal of research activity in design methodologies that explicitly account for structure and controller interactions. Some of the work has retained the traditional sequential design process, by focusing on methods to design structures that facilitate the performance of the controller (Haftka et al., 1985; Asada et al., 1991; O'Neal et al., 1998). However, such an approach is not truly integrated. In the ideal case, the problem would be posed as a single optimization problem, minimizing structural and control design variables simultaneously (McLaren and Slater, 1989; Rai and Asada, 1995). However, because of the nonconvex nature of the simultaneous problem, the numerical methods do not guarantee convergence. For this reason, methods that handle structural

---
*Author to whom correspondence should be addressed.
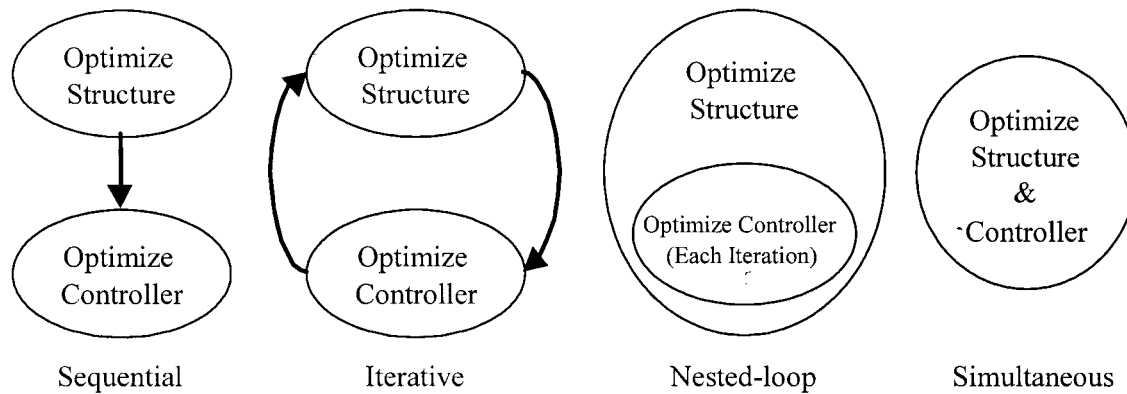Email: bkmin@umich.edu

Figure 1. Classifications of integrated structural/control design.

optimization and control optimization as two convex sub-problems have been developed. These methods are classified as iterative and nested-loop. The iterative methods solve a structural optimization sub-problem with a fixed controller and a controller optimization sub-problem with a fixed structure in multiple repeated steps (Khot et al., 1987; Kajiwara and Nagamatsu, 1991; Skelton and Kim, 1992; Smith et al., 1992; Park and Asada, 1994; Grigoridais et al., 1996; Shi et al., 1996). The nested-loop methods better leverage the work done by the control community, solving the controller optimization problem as a nested-loop at each iteration (step) of the structural optimization problem Figure 1.

Much of the research in the boring area has focused on vibration reduction related to either one of two sources: forced vibration (due to cutting forces and mass unbalance) or self-excited vibration (chatter). Studies to reduce vibration explore either passive or active methods.

Passive method using high elastic modulus materials, such as tungsten alloys and sintered carbide, directly improves boring bar stiffness. Rivin (1993) proposed a boring bar made of several layers of different materials to improve rigidity. However, these methods are uneconomical due to the material cost and do not improve damping characteristics. Rivin and Kang (1992) proposed a use of passive dynamic vibration absorber (DVA) to increase the damping of the bar. Boring bars with manually adjustable DVA which can be tuned for varying spindle speeds are currently commercially available. Lee et al. (1988) adopted a bar of graphite epoxy composite to improve both stiffness and damping. A replicated internal viscous damper in the core of boring bar to improve damping was introduced (Slocum et al., 1994). Andreassen (1995) devised an adjustable cylindrical damper for boring bars, in which ring-shaped elastic spring elements and damping oil provide the damping action. Nevertheless, all passive methods only improve boring accuracy to a certain level; further

improvement can be achieved only by using active vibration reduction approaches.

A number of research papers deal with boring bar designs involving active control. Tanaka et al. (1994) utilized an outer layer of piezoelectric material to generate damping forces in response to the vibration of the cutting insert. Boring bars with piezoelectric powered DVA were introduced (Tewani et al., 1988). Optimal state feedback (Tewani et al., 1991) and H_∞ control algorithm (Marra et al., 1995) were used to control the active DVA.

Several systems have been developed that are capable of moving the tool tip insert relative to the tool post for the purpose of on-line correction of systematic and pre-mapped machine errors (Kouno, 1982; Okazaki, 1990). Kim et al. (1987) proposed a boring bar with a laser-guided piezoelectric powered tool tip servo as a vibration isolation system. The system used Forecasting Compensatory Control (FCC) to construct an autoregressive stochastic model of the cylindricity error of the boring bar. A feed forward controller generated a control command to the piezoelectric actuator that was 180° out of phase with this forecasted error. However, since the piezoelectric actuator was not in the controller loop, tool tip was susceptible to hysteresis, drift, and cutting force disturbance errors. Rasmussen et al. (1992) introduced a fast tool servo to generate non-circular profiles. The effectiveness of a PID and repetitive control schemes were investigated. In addition, an analytical model was used for designing the fast tool servo. The work was extended by Hanson and Tsao (1994) using an inner-loop H_∞ controller in addition to the outer-loop repetitive controller. It has to be stressed, however, that most of the reviewed work focused on standard boring processes for which the L/D ratio of the bar did not exceed 5:1, or addressed similar applications, including turning.

This paper presents an integrated structure/control design methodology for the *Smart Tool*. This paper introduces new uses of covariance responses of the

system as objective and constraint functions. These objectives and constraints include not only performance and control force but also structural fatigue, buckling, and the time derivative of the control force. Both geometric dimensions and the controller gains are optimized simultaneously to minimize a single objective function. For the stated model of the *Smart Tool*, the objectives, constraints, and their sensitivities are solved in closed form.

SMART TOOL DESCRIPTION

The overall project goal was to develop a boring station with increased flexibility (Koren et al., 1999). The final design supports agility by enabling automated tool changes and providing an advanced on-line compensation mechanism. For machining of long bores, a process called line boring is employed; the name of the process refers to the consecutive machining of bores with the same diameter (such as in bearing nests). Such operations currently require dedicated manufacturing equipment and, hence, impede the achievement of full flexibility of machining systems.

One of the major obstacles to automated tool changes is that current tooling designs require an outboard and possibly intermediate support bearing, as shown in Figure 2. In the proposed solution, this bearing may be eliminated, but then use of a conventional tool leads to vibrations and problems with precision. The *Smart Tool* improves the dynamic stiffness of the boring bar relative to the spindle, eliminating the requirement of this support bearing. An overview of the Smart Boring Tool system layout is presented in Figure 3. The necessary instrumentation is located in the package attached to the rear end of the spindle and rotating with it. Note that the length of the tool extending out of the inboard support may vary.

The structure of *Smart Tool* is depicted in Figure 4. The *Smart Tool* consists of the following main
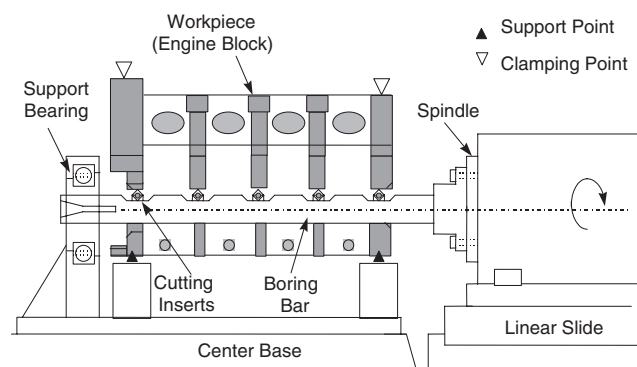
subsystems: (i) measurement system, (ii) computer controller, (iii) cutting insert, (iv) tool tip flexure mechanism, and (v) piezoelectric actuator.

i. Two position-sensitive optical detectors, measuring the position of the cutting insert and the end of the boring bar relative to the spindle, provide real-time feedback signals. The detector measuring the position of the cutting tool is a single-axis, bi-cell detector. The detector measuring the displacement of the end of the boring bar is a two-dimensional, continuous, position-sensitive detector. The one-dimensional and two-dimensional sensors used in the method have a sensitivity of about 1 μm. The use of position-sensitive optical detectors is based on the assumption that the motion of the precision spindle is negligible or deterministic.

ii. The controller is realized by a PC/104 computer (133 MHz AMD 5×86 CPU) and an off-the-shelf analog interface. All control algorithms are embedded in the controller using a memory IC and the control loop has a 0.15 ms sampling period. The *Smart Tool* controller communicates with the machine controller using a standard serial data port. The machine controller can start and stop the control loop, and upload and download data and parameters to and from the *Smart Tool*. Data and power are transmitted through a non-contact inductive connection.

iii. The tool is equipped with two cutting inserts: a rough cutter and a finish cutter. The rough cutter is attached directly to the boring bar, while the finish cutter is attached to the flexure mechanism, enabling its motion relative to the tool.

iv. A piezoelectric stacked actuator provides the actuation force to the flexure mechanism. This type of actuator was chosen for its large power-to-volume ratio and high operating frequency. A lever connecting the actuator with the tool tip translator allows the actuator to magnify its displacement.

v. The tool tip flexure mechanism enables rectilinear motion of the cutting insert in the depth of cut direction and provides preload to the piezoelectric actuator. The mechanism is dynamically balanced to reduce rotational effects.

MODELING *SMART TOOL* STRUCTURE

As described in previous section, *Smart Tool* is composed of several subsystems such as piezoelectric actuator, tool tip mechanism, and sensors. In this section, the mathematical models of piezoelectric actuator and tool tip mechanism are derived. The models include design variables, such as physical dimension of piezo-electric actuator, which directly affect the performance
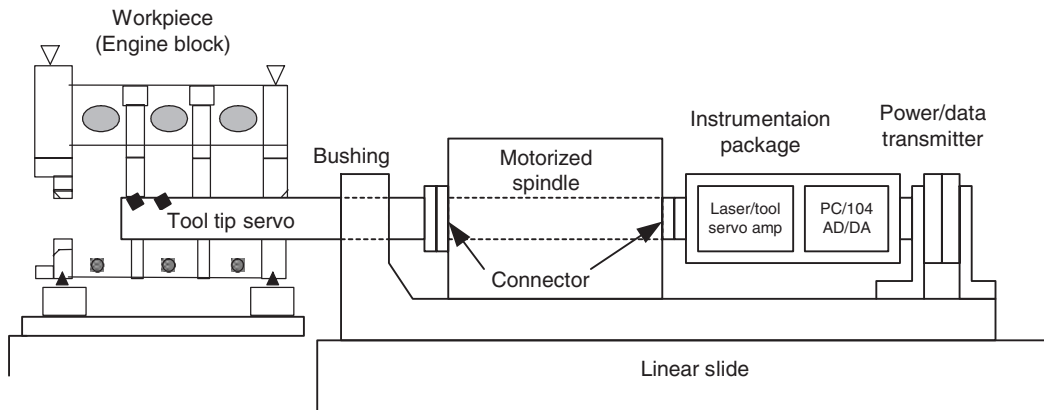
Figure 2. *Conventional line boring with outboard support and multiple cutting inserts.*

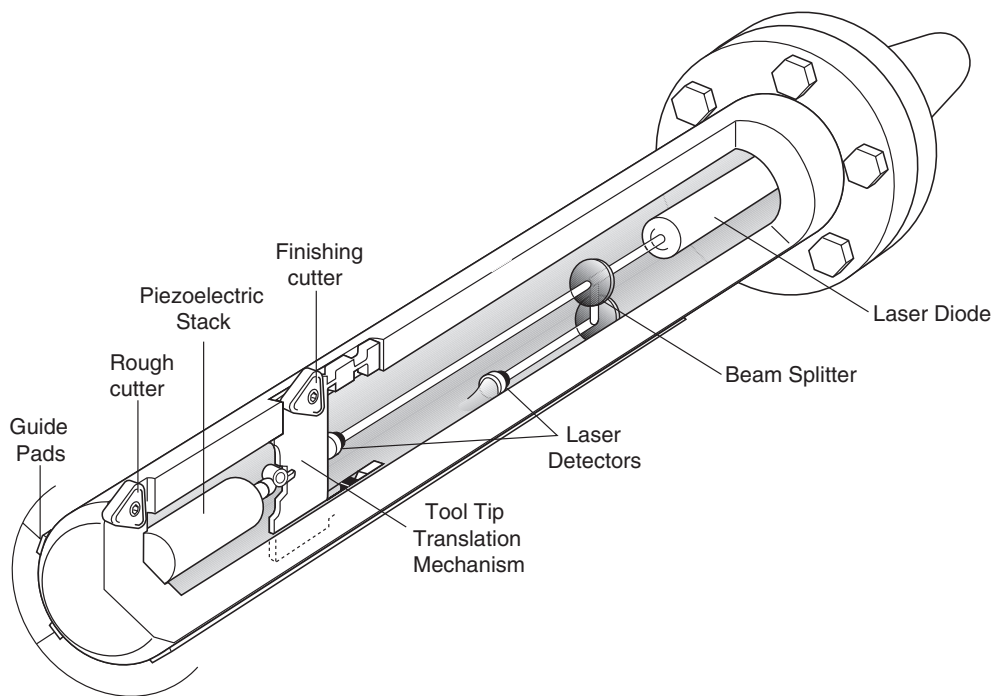**Figure 3.** Overview of Smart boring tool system.

Figure 4. Structure of Smart Tool.

of *Smart Tool*. The derivation of mathematical model is important because the design variable included in these models will be used for integrated structure/control design optimization described in the next section.

Piezoelectric Actuator

Piezoelectric material has the property of changing shape in an electric field, allowing it to be used as an electromechanical transducer. Detailed tool tip servo mechanism is depicted in Figure 5. A piezoelectric actuator behaves like a spring, with variable free length and distributed mass. The free length is approximately proportional to the applied voltage. The compression force generated in the piezoelectric actuator in the figure is approximated by the following formula:

$$F_p = -\frac{A_p Y_{33}^E}{l_p} \Delta x + A_p \frac{Y_{33}^E d_{33}}{t} V. \tag{1}$$

A_p, l_p, t, Y_{33}^E, d_{33} and Δx are the area, length, layer thickness, Young's Modulus, strain constant, and extension of the piezoelectric actuator, respectively (see Figure 5). Equation (1) assumes the piezoelectric actuator has negligible mass, hysteresis, and drift. The two terms of Equation (1) are the stiffness of the piezoelectric actuator and the control force, respectively. The control force, a function of the voltage (V) supplied
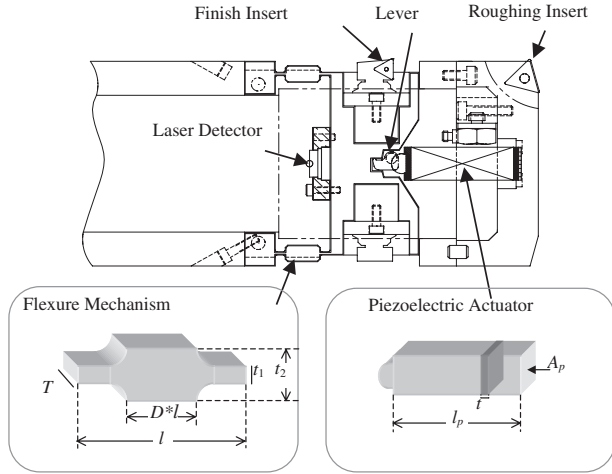
Figure 5. Details of tool tip servo mechanism.

by the power amplifier, is subject to saturation in both amplitude and time rate of change. These nonlinearities are functions of the piezoelectric material and power amplifier properties. Piezoelectric material begins to depolarize under the influence of strong electric fields, promoting manufacturers to specify a maximum allowable electric field. This corresponds to a maximum voltage (V_{max}) for a given piezoelectric layer thickness. The maximum actuator force is limited by:

$$\max(f_a) = A_p \frac{Y_{33}^E d_{33}}{t} V_{max}. \quad (2)$$

Power amplifiers are also subject to voltage saturation, which may be the limiting factor determining V_{max}. The saturation current of the power amplifier and piezoelectric property limits the time rate of change of the control force, as demonstrated by the following equation:

$$\max(\dot{f_a}) = \frac{t Y_{33}^E d_{33}}{\varepsilon_o K_{33}^T} \frac{I_{max}}{l_p}, \quad (3)$$

where ε_o is the permittivity of free space and K_{33}^T is the piezoelectric dielectric constant.

The piezoelectric actuator is subjected to high compressive forces, which can be estimated using Equation (1). Compression force may lead to a crucial value $F_{critical}$ at which buckling occurs; hence, F_p has to be constrained. The constraint can be found via the optimization algorithm.

Tool Tip Mechanism

The proposed tool tip mechanism design is utilizing flexure (see Figure 5). The stiffness to an actuating

force (K_l) is estimated by the following equation:

$$K_l = 2 \frac{ET}{l^3} \left(\left(\frac{1}{t_2^3} - \frac{1}{t_1^3} \right) D^3 + \frac{1}{t_1^3} \right)^{-1}, \quad (4)$$

where E, T, l and t_1 are the elastic modulus, width, length, and thickness of the flexure. The flexure has a thicker cross-sectional area in its middle section, which increases the ratios of the compliance in the drive direction to the perpendicular directions. D is the ratio of the length of this center section to that of the entire flexure; t_2 is the thickness of this center section.

The flexure mechanism must withstand the motion of the cutting insert and provide a preload to the piezoelectric actuator without fatiguing. A constraint involving the alternating and mean stresses provides a factor of safety against fatigue (see Equation (23)). The mean stress is assumed to arise from the piezoelectric preload and the alternating stress from the motion of the flexure mechanism, ignoring the influence of cutting forces. Under these assumptions, the mean (σ_m) and alternating (σ_a) components of the principal stress are:

$$\sigma_m = \frac{3l}{2t_1^2 T} \max(f_a) \quad \text{and} \quad \sigma_a = \frac{3l K_l}{2t_1^2 T} (\Delta x). \quad (5)$$

This assumes the preload to be half the maximum control force, allowing equal control force in both directions of the tool tip motion. Δx is the motion of the tool tip mechanism relative to the tool which will be evaluated closed loop.

System Model

The bar and tool tip flexure mechanism can be modeled as mass-spring-damper systems as described in Appendix A.1. The model is written in standard notation like:

$$\dot{\mathbf{X}} = \mathbf{A_o X} + \mathbf{B_o f_a} + \mathbf{B_c f_d}$$

$$\mathbf{Y} = \begin{bmatrix} \mathbf{C_o} \\ \mathbf{C_b} \\ \mathbf{C_s} \end{bmatrix} \mathbf{X}. \quad (6)$$

One should assume direct, full-state feedback of the form $f_a = -\mathbf{KX}$. The closed-loop dynamic equations are given by:

$$\dot{\mathbf{X}} = \mathbf{A_c X} + \mathbf{B_c f_d}, \quad (7)$$

where $\mathbf{A_c} = \mathbf{A_o} - \mathbf{B_o} \cdot \mathbf{K}$.

OPTIMIZATION PROBLEM FORMULATION

The main purpose of the *Smart Tool* is to minimize positional errors of the cutting insert. To this end, the optimization objective is to minimize the covariance of the cutting insert error in response to white noise cutting disturbances. The *Smart Tool* is subject to actuator saturation and structural integrity limitations. To limit actuator saturation, bounds are placed on the standard deviation of the control force and its time derivative in response to this same white noise disturbance. To limit fatigue, the standard deviation of the stroke of the flexure mechanism (Δx) is bounded. To help prevent buckling, standard deviation of the compressive load in the piezoelectric actuator is bounded. It is important to note that the bounds on these quantities themselves are specified as functions of the design variables.

Covariance Analysis

The objectives and constraints used in this paper were expressed in terms of steady-state covariance matrices. These covariance matrices can be computed explicitly from the solution to the algebraic Riccati Equation (Equation (9)). This proposed method is more convenient than expressing the objectives and constraints in terms of the time trajectory of the system because it does not require numerical method to solve differential equations (For example, imposing an upper bound on $u(t)$ requires time domain simulation.). Further Sequential Quadratic Programming (Powell, 1983) is used to solve this optimization problem, for which sensitivities of objectives and constraints are required. These sensitivities can be estimated numerically by perturbing the design variables, but this is computationally intensive. The covariance formulation makes it possible to derive all the sensitivities analytically.

The steady-state covariance ($E\{\mathbf{X}(t)\mathbf{X}^T(t)\}$) of a linear time-invariant asymptotically stable system subject to white noise disturbances can be found in the following way:

$$E\{\mathbf{X}(t)\mathbf{X}^T(t)\} = \mathbf{P}. \qquad (8)$$

where $\mathbf{P}$ is the unique positive-definite solution of the following algebraic Lyapunov equation:

$$\mathbf{A}_c\mathbf{P} + \mathbf{P}\mathbf{A}_c^T + \mathbf{B}_c\mathbf{Q}\mathbf{B}_c^T = \mathbf{0}, \qquad (9)$$

and $\mathbf{Q}$ is the disturbance covariance matrix ($E\{\mathbf{f}_d(t)\mathbf{f}_d^T(t)\}$) for the system. Equation (9) has a positive-definite solution if and only if $\mathbf{A}_c$ is asymptotically stable. For unstable systems, the state covariance matrix has infinite elements, assuming the system is controllable from the disturbance, yet Equation (9) has

negative-definite solutions. To avoid using this solution as the covariance of the states, the system has to be constrained to be asymptotically stable or, equivalently, $\mathbf{P}$ has to be positive definite. Such conditions can be assured by use of the Routh–Hurwitz criteria, since they yield constraints that could be solved in closed form. Directly constraining the eigenvalues of $\mathbf{A}_c$ to be negative definite and/or $\mathbf{P}$ to be positive definite requires solving a fourth-order polynomial, which in general has no closed-form solution. Second-order analysis $\mathbf{M}\ddot{\mathbf{X}} + \mathbf{B}\dot{\mathbf{X}} + \mathbf{K}\mathbf{X} = \mathbf{0}$ would require only solving a second order polynomial for the eigenvalues of the system, if the controller is used to enforce proportional damping (i.e. $\mathbf{B}$ is a scalar multiple of $\mathbf{M}$ and $\mathbf{K}$).

The covariance matrix is used to evaluate the covariance of an output response (y). If the output is of the form:

$$y = \mathbf{C}_y\mathbf{X}. \qquad (10)$$

where $\mathbf{C}_y$ is an output matrix, then the covariance of this response becomes:

$$E\{y(t)^2\} = \mathbf{C}_y\mathbf{P}\mathbf{C}_y^T. \qquad (11)$$

The standard deviation of this response (σ_y) is obtained by taking the positive square root:

$$\sigma_y = \sqrt{\mathbf{C}_y\mathbf{P}\mathbf{C}_y^T}. \qquad (12)$$

If the input to a linear system follows a Gaussian distribution, then the output response will also follow a Gaussian distribution (Papoulis, 1965). This allows the response to be quantified in terms of confidence intervals. If the output has a maximum allowable value ($\max(y)$), $w\cdot$(standard deviations of the output) can be constrained to be less than or equal to this maximum value, by a constraint of the form:

$$w\sqrt{\mathbf{C}_y\mathbf{P}\mathbf{C}_y^T} \leq \max(y). \qquad (13)$$

The weighting function (w) can be used to specify the minimum percentage of the time a condition must be satisfied. It can also be interpreted as a weighting function to balance an inherent tradeoff in the system design. For example, in the fatigue constraint, w can be used to balance the tradeoff between performance and life expectancy.

A problem arises in use of Equation (13), because SQP does not remain inside the feasible domain at each iteration. During iterations where the constraints on the stability of the closed loop system are not satisfied, Equation (13) will incorrectly give negative values for the covariance of the output response. It was found

that using the absolute value of the results obtained from Equation (13) helped the convergence of the optimization problem.

Formulating Objectives and Constraints

The formulation of objectives and constraints is consistent with the covariance analysis of the previous section. The objective is to minimize the covariance of the error in cutting insert position. This error is given by $y_o = \mathbf{C}_o\mathbf{X}$, when the insert is on the flexure mechanism (finish cutter), and by $y_b = \mathbf{C}_b\mathbf{X}$, when it is on the tool (rough cutter). These outputs are expressed in the form of Equation (12), therefore, the objective is to minimize:

$$J = w_o\mathbf{C}_o\mathbf{P}\mathbf{C}_o^T + w_b\mathbf{C}_b\mathbf{P}\mathbf{C}_b^T, \tag{14}$$

where w_o and w_b are weighting functions. The control force $(f_a = -\mathbf{K}\mathbf{X})$ has a maximum value given by Equation (2). Therefore, consistent with Equation (13), the following constraint limits actuator saturation:

$$w_s\sqrt{\mathbf{K}\mathbf{P}\mathbf{K}^T} \leq \max(f_a). \tag{15}$$

The time rate of change in the control force $(\dot{f}_a = \partial(-\mathbf{K}\mathbf{X})/\partial t)$ for fixed feedback gains is given by:

$$\dot{f}_a = -\mathbf{K}\dot{\mathbf{X}} = -\mathbf{K}\mathbf{A}_c\mathbf{X} - \mathbf{K}\mathbf{B}_c\mathbf{f}_d. \tag{16}$$

For linear systems with no direct feed through term, the states of the system are uncorrelated with white noise disturbance. Therefore, the covariance of $\dot{f}_a$ is equal to the sum of the covariances of the individual terms in Equation (16). The first term is of the form of Equation (12), and the covariance of $\mathbf{f}_d$ is known. The time rate of change has a maximum value given by Equation (3). Therefore, consistent with Equation (13), the following constraint limits actuator rate saturation:

$$w_r\sqrt{\mathbf{K}\mathbf{A}_c\mathbf{P}\mathbf{A}_c^\mathbf{T}\mathbf{K}^\mathbf{T} + \mathbf{K}\mathbf{B}_c\mathbf{Q}} \leq \max(\dot{f}_a). \tag{17}$$

A fatigue constraint for the thin portion of the flexure mechanism places an upper limit on the stroke $(\Delta x_{\text{fatigue}})$, as given in Equation (24). Since $\Delta x = \mathbf{C}_s\mathbf{X}$, then, consistent with Equation (13), the following constraint limits fatigue:

$$w_f\sqrt{\mathbf{C}_s\mathbf{P}\mathbf{C}_s^T} \leq \Delta x_{\text{fatigue}}. \tag{18}$$

A buckling constraint of the piezoelectric actuator places a limit on the compressive force F_{critical}, as given in Equation (25). The compressive force in the

actuator is obtained in the form of Equation (10), by applying the control law to Equation (1):

$$F_p = -\left(\frac{A_p Y_{33}^E}{l_p}\mathbf{C}_s + \mathbf{K}\right)\mathbf{X}. \tag{19}$$

Therefore, consistent with Equation (13), the following constraint must be in force to help prevent buckling:

$$w_b\sqrt{\left(\frac{A_p Y_{33}^E}{l_p}\mathbf{C}_s + \mathbf{K}\right)\mathbf{P}\left(\frac{A_p Y_{33}^E}{l_p}\mathbf{C}_s + \mathbf{K}\right)^T} \leq F_{\text{critical}}. \tag{20}$$

NUMERICAL RESULTS

Numerical Optimization Conditions

The optimization problem was solved using SQP. The *Smart Tool* was designed to make rough and finish cuts in a single pass, but not simultaneously. The structural parameters must remain fixed, while the controller can change depending on which insert is cutting. This is the reason for the two sets of control gains in Table 1. The weights on the objective function balance a performance tradeoff in rough versus finish cuts. All of the constraints must hold for both cases, a situation which doubles the number of constraints. The design variables were chosen carefully to simplify the optimization problem. The stiffness of the piezoelectric actuator, flexure mechanism, and feedback gain on Δx (k_3), which act in parallel, is specified as the design variable K_t, defined by:

$$K_t = K_p + K_l + k_3 \tag{21}$$

This formulation helps simplify the solution of the covariance matrix; the solution of the algebraic

Table 1. Design variables.

Structural		Controller		
		Flexure Mechanism		**Tool**
Piezoelectric area	A_{pe}	Feedback on		Feedback on
Piezoelectric length	l_{pe}	Bar position	k_{1o}	Bar position	k_{1b}
Lever gear ratio	gr	Bar velocity	k_{2o}	Bar velocity	k_{2b}
Flexure mechanism thickness	t_1	Stroke velocity	k_{4o}	Stroke velocity	k_{4b}
		Effective stiffness	K_{to}	Effective stiffness	K_{tb}

Lyapunov Equation (9) is no longer a function of the piezoelectric or flexure mechanism characteristics. This has the additional effect of reducing the number of nonzero sensitivities.

The actual cross-sectional area and length of the piezoelectric actuator are not design variables. Rather the effective area and effective length are specified as design variables. By *effective* we mean the length and area that has the equivalent effect on the system assuming unit gear ratio of the lever. Assuming the hinge of the lever is rigidly linked to the base of the piezoelectric actuator, an equivalent area (A_{pe}) and length (l_{pe}) are given respectively by:

$$A_{pe} = \frac{A_p}{gr} \quad \text{and} \quad l_{pe} = l_p gr. \qquad (22)$$

By *equivalent*, we meant that the stiffness and saturation remain the same, but not the buckling characteristics. This allows the optimization problem to be decoupled. First, the problem can be solved assuming unit-gear ratio and no buckling, and then the gear ratio can be chosen to satisfy the buckling constraint.

The fatigue in the flexure mechanism is estimated using the Goodman fatigue formula (Shigley, 1986) stated as follows:

$$\frac{\sigma_m}{S_{ut}} + \frac{\sigma_a}{S_e} = \frac{1}{FS}. \qquad (23)$$

This fatigue constraint is correlated to a limit on Δx, by substituting Equations (2) and (5) for Equation (23) yielding:

$$\Delta x_{\text{fatigue}} = \frac{2t_1^2 TS_e}{3lK_l FS} - \frac{A_p Y_{33}^E d_{33} S_e V_{\max}}{tK_l S_{ut}}. \qquad (24)$$

This is used in the fatigue constraint of Equation (20).

For a non-rotating tool, the critical force causing buckling in the piezoelectric actuator is predicted using Euler's formula (Beer and Johnston, 1979), which assumes both ends are pinned. The bar rotation (W_o) causes a moment due to centripetal acceleration, in addition to the moment from the compressive force accounted for by Euler's formula. This force, like the compressive force, establishes moments in the piezoelectric actuator that are a function of the bending of the piezoelectric actuator. To accurately account for this phenomenon requires solving a nonlinear differential equation, to determine the deformation shape of piezoelectric actuator under buckling. But assuming the piezoelectric actuator has the same deformation shape with purely compressive force buckling can approximate the effect. In this case, the critical

compressive force is given by:

$$F_{\text{critical}} = \frac{\pi^2 Y_{33}^E A_p^2}{0.0012 l_p^2} - 0.0026 \, W_o^2 m_p l_p^2 A_p - A_p \frac{Y_{33}^E d_{33}}{t} V_{\max} \qquad (25)$$

Results and Discussion

The simultaneously optimized structure/controller designs are compared with the original *Smart Tool*. The controller for the original tool was designed with the same objectives and constraints as the simultaneous optimization; only the structure parameters were fixed. The structure of the original *Smart Tool* was designed using a more traditional approach (O'Neal et al., 1998).

Figure 6 compares controller performance of the original *Smart Tool* with the simultaneously optimized design based on the cutting insert position error as a function of the length-to-diameter ratio of the tool. These results are for the parameters given in Table 2, and represent equal weighting on rough and finish cuts ($w_o = w_b$). The performance is compared by $2\sigma_e$ error in cutting insert position, hence the area under the plots can be interpreted as 95.4% confidence intervals for the absolute value of the error. The line at $5\,\mu m$ represents the maximum allowable error (not allowable σ_e) to produce quality parts. The simultaneous design is considerably more precise than the original design, especially at larger length-to-diameter ratios. In fact, the maximum allowable error during finish cuts of $5\,\mu m$ remains in the 95.4% confidence interval about 40% longer with the simultaneous design than with the original design. For rough cuts, the number is 30%. It must be noted that design of *Smart Tool* boring bar and
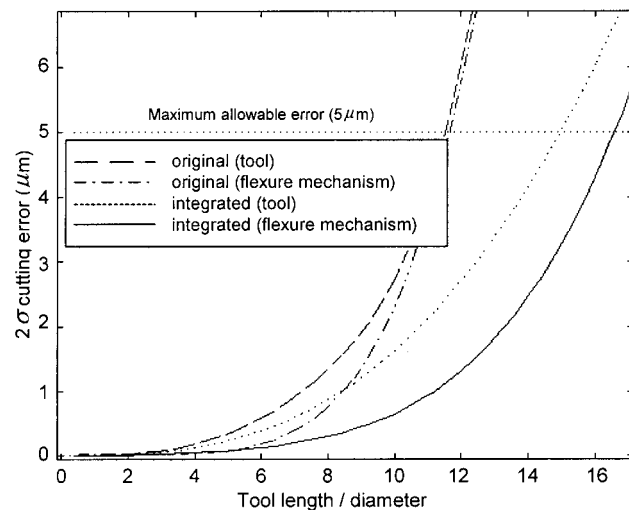
Figure 6. Comparison of cutting insert position error of original *Smart Tool* design vs. simultaneous structure/controller design.

Table 2. Model parameters in standard metric units.

| Piezoelectric Material & Amplifier		Translation Mechanism		Boring Tool		Standard Deviations & Safety Factors	
Young's modulus Y_{33}^E	4.8×10^{10}	Width T	0.025	Moment of inertia I	7.1×10^{-7}	Saturation f_a	3
Dielectric constant K_{33}^T	3400	Mass M_m	0.15	Young's modulus E_b	2×10^{11}	Rate saturation $\dot{f_a}$	3
Strain constant d_{33}	5.5×10^{-8}	Length l	0.016	Ultimate strength S_{ut}	1.4×10^{11}	Fatigue w_f	3
Max. voltage V_{max}	100	Damping b_m	0	Damping b_b	0	FS	2
Density m_p	7500	Length $D.l$	0.01	Yield strength S_e	3.4×10^{10}	Buckling w_b	3
Max. current I_{max}	2	Young's modulus E	2×10^{11}	Covariance cutting force	4		
				Spindle speed W_o	100 Hz		
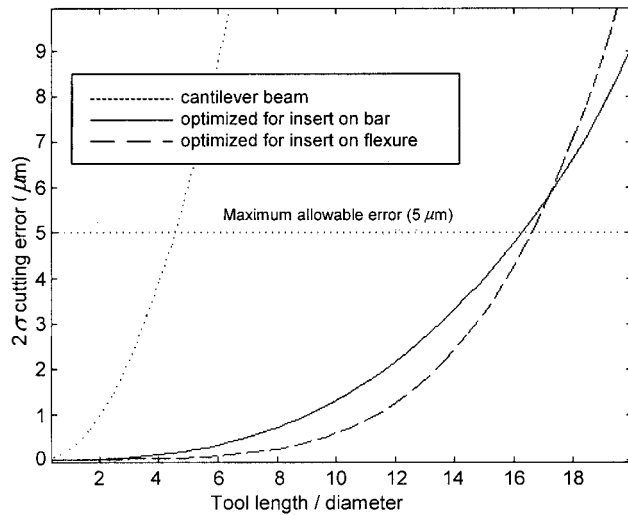
Figure 7. Performance with insert on flexure mechanism vs. insert on tool.

cutting conditions used to present this result were selected to meet non-chatter conditions. Readers interested in chatter analysis of *Smart Tool* are recommended to refer Li et al. (1998) and Li (1999).

The insert on the flexure mechanism exhibits better performance than the insert on the tool, for both the original and simultaneous designs. For the original tool, this may be an artifact relating to the insert on the flexure. For the simultaneous design, this could be explained the choice of the objective weights. A better understanding of the inherent limits in the system is obtained by optimizing two separate designs: for the insert on the flexure mechanism (i.e., $w_b = 0$) and for the insert on the tool (i.e., $w_o = 0$). Figure 7 suggests that the system performs best with the cutting insert on the flexure mechanism, up to a certain length-to-diameter ratio, after which designs with the insert directly on the tool have lower errors.

For these design parameters this does not occur until the length-to-diameter ratio is about 17, and the maximum allowable error is outside the 95.4% confidence interval. For comparative purposes, results for a cantilever beam using Equation (A.1) in Appendix and a damping ratio of 0.003 are also given.
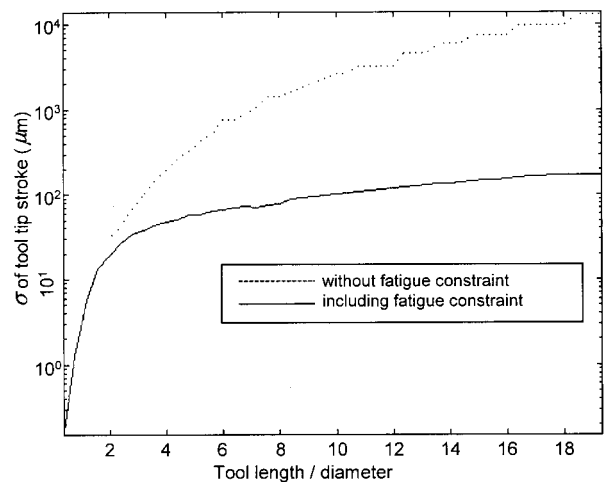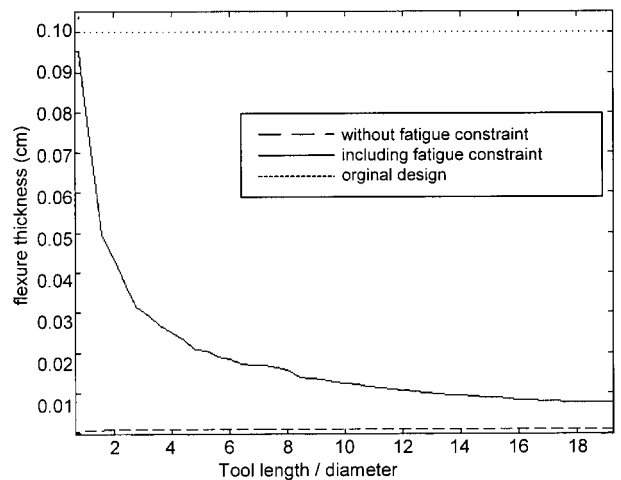

Figure 8. Optimal solution with fatigue constraint removed.

One of the objectives of this paper is to introduce new uses for steady-state covariance information, namely using it to limit fatigue, buckling, and saturation in the time derivative of the control force. These constraints were removed one at a time to evaluate their effects on the optimal solution. If the fatigue constraint Equation (18) is removed, the optimal value for t_1 becomes zero while the stroke (Δx) becomes very large. The results for the insert on the bar are shown in Figure 8. If the buckling constraint is removed, then the piezoelectric
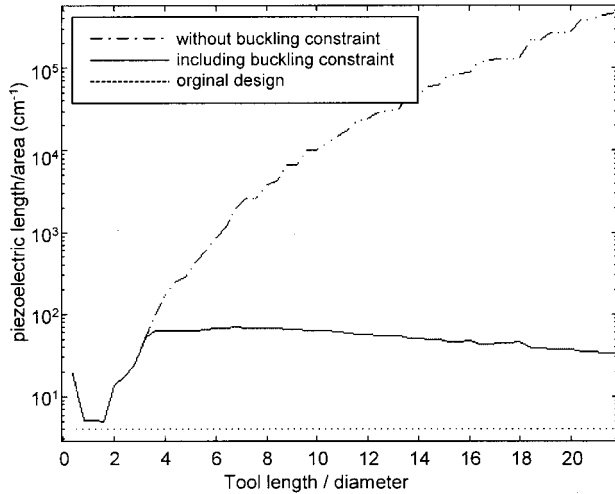
Figure 9. *Optimal solution with buckling constraint removed.*

actuator requires a very large length-to-diameter ratio, which is physically unreasonable. (See Figure 9.)

When the constraint on the time derivative of the control force Equation (17) is eliminated, convergence problems occur, so no results are given for that case. The system has an inherent trade-off in the length of l_p, which is lost when this constraint is removed. The longer the piezoelectric actuator, the greater the stroke, but also the greater the capacitance, which is given by:

$$c = \frac{l_p A_p K_{33}^E \varepsilon_o}{t^2}. \qquad (26)$$

The larger the capacitance, the more current is required to have the same time derivative of the control force. This tradeoff is lost, though, if this constraint is removed, and the objective is minimized at l_p equal to infinity.

CONCLUSIONS

An integrated structural/control optimization approach has been formulated and applied to the design of a micro-positioner for a boring bar tool insert. Covariance responses of the system were used as objective and constraint functions. It was shown that covariance analysis can be applied beyond just performance and control force. This extension allows for accommodation of non-traditional constraints: structural fatigue, buckling, and the time derivative of the control force. These constraints proved very useful in obtaining viable design solutions. The methodology extended the range of feasible designs: e.g., a boring tool of up to 40% longer length that still maintains the allowable error inside the 95.4% confidence interval.

APPENDIX

Smart Tool Model

The model for the *Smart Tool* used in the optimization algorithm is shown in Figure A.1. The bar and flexure mechanism are modeled as mass-spring-damper systems. A first-mode approximation of a boring bar is obtained by assuming the bar to be a fixed-free cantilever beam (Thomson, 1993). The natural frequency (w_n), equivalent stiffness (K_b), and equivalent mass (M_b) of the first mode of a cantilever beam are approximated by:

$$w_n = 3.52\left(\frac{EI}{m_b \cdot l_b^4}\right)^{0.5} \quad K_b = 3\frac{EI}{l_b^3} \quad M_b = \frac{K_b}{w_n^2}. \quad (A.1)$$

where m_b, l_b, E_b, and I are the mass per unit length, length, elastic modulus, and area moment of inertia of the boring bar. The following is a state-space representation of this system:

$$\frac{\partial}{\partial t}\begin{bmatrix} x_b \\ \dot{x}_b \\ \Delta x \\ \Delta \dot{x} \end{bmatrix}$$

$$= \begin{bmatrix} 0 & 1 & 0 & 0 \\ -\dfrac{k_b}{M_b} & -\dfrac{b_b}{M_b} & \dfrac{K_p+K_l}{M_b} & \dfrac{b_m}{M_b} \\ 0 & 0 & 0 & 1 \\ \dfrac{k_b}{M_b} & \dfrac{b_b}{M_b} & -(K_p+K_l)\left(\dfrac{1}{M_b}+\dfrac{1}{M_m}\right) & -b_m\left(\dfrac{1}{M_b}+\dfrac{1}{M_m}\right) \end{bmatrix}$$

$$\times \begin{bmatrix} x_b \\ \dot{x}_b \\ \Delta x \\ \Delta \dot{x} \end{bmatrix} + \begin{bmatrix} 0 \\ \dfrac{1}{M_b} \\ 0 \\ -\left(\dfrac{1}{M_b}+\dfrac{1}{M_m}\right) \end{bmatrix} \cdot f_a + \begin{bmatrix} 0 & 0 \\ 0 & \dfrac{1}{M_b} \\ 0 & 0 \\ -\dfrac{1}{M_m} & -\dfrac{1}{M_b} \end{bmatrix} \cdot \begin{bmatrix} f_c \\ f_b \end{bmatrix}$$

$$\begin{bmatrix} y_o \\ y_o \\ \Delta x \end{bmatrix} = \begin{bmatrix} 1 & 0 & 1 & 0 \\ 1 & 0 & 0 & 0 \\ 0 & 0 & 1 & 0 \end{bmatrix} \begin{bmatrix} x_b \\ \dot{x}_b \\ \Delta x \\ \Delta \dot{x} \end{bmatrix}, \qquad (A.2)$$

where $\Delta x = x_m - x_b$.

f_c

Flexure mechanism
(M_m)

x_m

actuator force (f_a) K_p K_l b_m
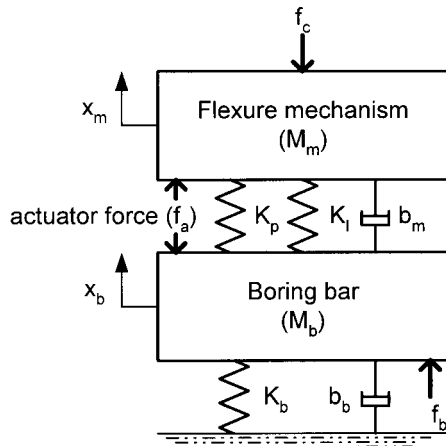
x_b

Boring bar
(M_b)

K_b b_b f_b

Figure A.1. *Model of Smart Tool.*

REFERENCES

Andreassen, L. (1995). Means for damping vibrations for example self-generated oscillations in boring bars and similar. U.S. Pat. 5413318.

Asada, H., Park, J.-H., Rai, S. (1991). A control-configured flexible arm: integrated structure/control design. In: *Proceedings IEEE International Conf. on Robotics and Automation*. Sacramento, pp. 2356–2362.

Beer, F. and Johnston, E. (1979). *Mechanics of Materials*. New York: McGraw Hill. pp. 526–529.

Grigoriadis, K., Zhu, G. and Skelton, R. (1996). Optimal redesign of linear systems. *ASME Journal of Dynamic, Systems, Measurement and Control*. **118**: 598–605.

Haftka, R.T., Martinovic, A.N. and Hallauer W.Jr., (1985). Enhanced vibration controllability by minor structural modifications. *AIAA Journal*, **23**: 1260–1266.

Hanson, R.D. and Tsao, T. (1994). Development of a fast tool servo for variable-depth-of-cut machining. In: *Proc. ASME International Mechanical Engineering Congress and Exposition* DSC-Vol. 55-2. Dynamic Systems and Control: Vol. 2. pp. 863–871.

Kajiwara, I. and Nagamatsu, A. (1991). An approach to simultaneous optimum design of structure and control systems by sensitivity analysis. *ASME, DE-Vol. 38, Modal Analysis, Modeling, Diagnostics, and Control – Analytical and Experimental*. pp. 179–184.

Khot, N.S., et al. (1987). Optimal structural design with control gain norm constraint. *AIAA Journal*, **26**(5): 604–611.

Kim, K., Eman, K.F. and Wu, S.M. (1987). In-process control of cylindricity in boring operations. *Journal of Engineering for Industry*, **109**: 291–296.

Koren, Y., Pasek, Z. and Szuba, P. (1999). Design of a precision, agile line boring station. *CIRP Annals – Manufacturing Technology*, **48**(1): 313–316.

Kouno, E. (1982). A fast response piezoelectric actuator for a servo correction of systematic errors in precision machining. *CIRP Annals – Manufacturing Technology*, **33**(1): 369–372.

Lee, C.W., Katz, R., Ulsoy, A.G. and Scott, R.A. (1988). Modal analysis of a distributed parameter rotating shaft. *Journal of Sound and Vibration*, **122**(1): 119–130.

Li, C.-J., Ulsoy, A.G. and Endres, W. (1998). The effect of tool rotation on regenerative chatter in line boring. In: *Proceedings of Symposium on Dynamics, Acoustics, and Simulation, ASME IMECE*. DE-Vol. 98. pp. 235–243.

Li, C. (1999). Tool-tip displacement measurement, process modeling, and chatter avoidance in agile precision line boring. PhD Dissertation, The University of Michigan, Ann Arbor, MI.

Marra, M.A., Walcott, B.L., Rouch, K.E. and Tewani, S.G. (1995). H_∞ vibration control for machining using active dynamic absorber technology. In: *Proceedings of the American Controls Conference*. pp. 739–743.

McLaren, M. and Slater, G. (1989). A disturbance based control/structure design algorithm. In: *Proceedings of the 3rd Annual Conf. on Aerospace Computational Control*. Oxnard, CA. August 28–30.

Okazaki, Y. (1990). A micro-positioning tool post using a piezoelectric actuator for diamond turning machines. *Precision Engineering*, **12**(3): 151–156.

O'Neal, G., Min, B.-K., Li, C.-J., Pasek, Z.J., Koren, Y. and Szuba, P. (1998). Precision piezoelectric micro-positioner for line boring bar tool insert. In: *Proceedings of ASME International Mechanical Engineering Congress and Exposition, Vibration and Noise Control*. DSC-Vol 65. pp. 99–106.

Papoulis, A. (1965). *Probability, Random Variables, and Stochastic Processes*. New York: McGraw-Hill.

Park, J.-H. and Asada, H. (1994). Concurrent design optimization of mechanical structure and control for high speed robots. *ASME J. of Dynamic, Systems, Measurement and Control*, **117**: 344–354.

Powell, M.J.D. (1983). Variable metric methods for constrained optimization. *Mathematical Programming: The State of Art*, Springeer Veriza. pp. 288–311.

Rai, S. and Asada, H. (1995). Integrated structure/control design of high speed flexible robots based on time optimal control. *ASME, Journal of Dynamic Systems, Measurement, and Control*, **177**: 505–512.

Rasmussen, J.D., Tsao, T.C., Hanson, R.D. and Kapoor, S.G. (1992). A piezoelectric tool servo system for variable depth of cut machining. *PED-Vol. 58, Precision Machining: Technology and Machined Development and Improvement*. ASME.

Rivin, I.I. (1983). A chatter-resistant cantilever boring bar. In: *Proceedings of 11th North American Manufacturing Research Conference*. SME. pp. 403–407.

Rivin, E.I. and Kang, H. (1992). Enhancement of dynamic stability of cantilever tooling structures. *Intl. J. of Machine Tools & Manufacture*, **32**(4): 539–561.

Shi, G., Skelton, R. and Grigoriadis, K. (1996). Algorithms to integrate structure and control design. In: *Proceedings of IEEE International Symposium on Computer-Aided Control System Design*. Dearborn, MI.

Shigley, J.E. (1986). *Mechanical Engineering Design*. New York: McGraw Hill.

Skelton, R. and Kim, J. (1992). The optimal mix of structure redesign and active dynamic controllers. In: *Proc. ACC*. pp. 2775–2779.

Slocum, A.H., Marsh, E.R. and Smith, H.D. (1994). A new damper design for machine tool structures: the replicated internal viscous damper. *Precision Engineering*, **16**(3): 174–183.

Smith, M., Grigoriadis, K. and Skelton, R. (1992). Optimal mix of passive and active control in structures. *AIAA Journal of Guidance, Control and Dynamics*, **15**(4): 912–919.

Tanaka, H., Obata, F., Matsubara, T. and Mizumoto, H. (1994). Active chatter suppression of slender boring bar using piezoelectric actuators. *JSME International Journal, Series C*, **37**(3): 601–606.

Tewani, S.G., Rouch, K.E. and Walcott, B.L. (1988). Control of machining chatter by use of active elements. In: *Proc. Symp. on Advanced Manufacturing*. Univ. of Kentucky, Lexington, KY. pp. 31–36.

Tewani, S.G. (1991). Active optimal vibration control using dynamic absorber. In: *Proc. of IEEE Intl. Conf. on Robotics & Automation*. Sacramento, CA. pp.1182–1187.

Thomson, W.T. (1993). *Theory of Vibration with Applications*. Prentice-Hall.